Preprints of the 20th World Congress
The International Federation of Automatic Control
Toulouse, France, July 9-14, 2017

The Effect of Viscosity on the Maximisation of Electrical Power from a Wave Energy Converter under Predictive Control

Adrian C.M. O'Sullivan * **Gordon Lightbody** *

* *MaREI SFI Research Centre, University College Cork,Ireland (e-mail: adrian.osullivan@umail.ucc.ie).*

Abstract: In this paper, the non-linear effects of viscosity on the performance of a Wave Energy Converter (WEC) system are analysed. A standard linear Model Predictive Control (MPC) is used to show the negative effects that the unaccounted non-linear viscosity force in the hydrodynamic system has on the power absorption. A non-linear MPC (NLMPC) is then implemented, where the non-linear viscosity effects are included in the optimisation. A linear drag coefficient estimate of the non-linear viscosity is then included in the linear MPC; creating a Linear Viscous Model Predictive Control. When constraints are incorporated, it is shown that a single choice of the linear viscous drag coefficient for use within the linear MPC can provide comparable results to the non-linear MPC approach, over a wide range of sea states.

Keywords: MPC, LPV-MPC, power maximisation, viscosity, wave energy.

1. INTRODUCTION

In recent times there has been a renewed interest in wave energy, due primarily to the drive to replace fossil fuels in an attempt to combat climate change. As a renewable source, wave energy in particular is seen as attractive due to its high energy density, (Clément et al., 2002). There are numerous wave energy converter (WEC) paradigms which can extract this energy from the wave in various ways, and can operate either in the near shore or at offshore locations, (Drew et al., 2009). This work focuses on a point absorber wave energy converter, which is relatively simple from a mechanical point of view and which is applicable for wave farm arrays, (Budal and Falnes, 1975).

Incorporating control into the WEC is crucial for maximum power extraction and to protect the device. Classical control methods such as reactive control, (Budal and Falnes, 1977) and latching, (Budal and Falnes, 1980) have been used to extract maximum or close to maximum average power. The effect of system constraints have been investigated, (Fusco and Ringwood, 2013) as well as the use of a realistic non-ideal Power Take Off (PTO), (Tedeschi et al., 2011). Both latching and reactive control were originally designed to operate in monochromatic seas, however, there have been attempts to extend their use for irregular sea conditions, (Fusco and Ringwood, 2011; Babarit et al., 2004).

Other advanced control methods have been investigated; such as fuzzy logic, (Schoen et al., 2011), bang-bang control, (Abraham and Kerrigan, 2013), pseudo spectral control, (Paparella and Ringwood, 2016) and model predictive control (MPC), (Hals et al., 2011). In this paper MPC is utilised as the control algorithm due to its ability to produce optimal results, whilst easily incorporating system constraints within the optimisation, (Maciejowski, 2002). In the most commonly used MPC approach for wave energy, the average power is maximised over a certain prediction horizon based on a model of the device, (Cretel et al., 2010). When the PTO is included in the system, (Polinder et al., 2004), a cascade control scheme can be easily implemented, where the slower outer loop sends piecewise linear reference points to the faster inner PTO force control loop, (Montoya Andrade et al., 2014; Cretel et al., 2011). In (O'Sullivan and Lightbody, 2015), it is shown that it is essential to include the PTO power losses within the cost function, as the average power can dramatically reduce when the WEC operates away from its natural frequency.

It is crucial that each design aspect of the power extraction system from wave-to-wire is designed in an integrated manner, rather than as individual subsystems. This subject of co-design has lately been highlighted, where items such as the sea spectrum suitability, (Lenee-Bluhm et al., 2011), the geometry of the WEC, (Garcia-Rosa and Ringwood, 2016), the prediction of the excitation wave, (Fusco and Ringwood, 2010), the rating of the generator, (Aubry et al., 2012), the power electronics needed for high power ratings, (Lovelace et al., 2000), the effects of the DC-link on the power extraction, (O'Sullivan and Lightbody, 2016a,b) and the aggregation of power from multiple WEC's, (Molinas et al., 2007) have been analysed. One category that has been somewhat assumed as insignificant in previous wave energy research, is the importance of including and modelling the non-linear components of the WEC system. The main non-linearity in the hydrodynamic system are the Froude-Krylov forces and the viscosity forces. In both, (Guérinel et al., 2011; Penalba Retes et al., 2015), the effects of including non-linear Froude-Krylov forces in the hydrodynamics model were demonstrated.

Whilst in, (Bhinder et al., 2011; Giorgi et al., 2016), it was shown that without the implementation of active control, the effects on the power extraction is insignificant. However, when active control is used, the performance from the non-linear model considerably diverges from the linear model, (Giorgi et al., 2016).

In this paper, the non-linear effects of viscosity on the average power absorption are investigated. It first investigates the effect that unmodelled viscosity within the WEC has on the electrical power absorption when a linear model is used within the MPC. A non-linear MPC approach based on the linear parameter-varying (LPV) method is then utilised, in which the non-linear viscosity effect is approximated within the predictive model at each prediction step. This is further simplified, utilising a linear viscous damping within the predictive model, which is optimally tuned for each sea state. When constraints are included, it is shown that the electrical power extracted in our example was actually quite insensitive to the choice of the linear viscous damping coefficient and performance close to that obtained using the non-linear MPC could be obtained across all sea states, without the added computational complexity of the non-linear MPC.

2. MODELLING

2.1 Hydrodynamics

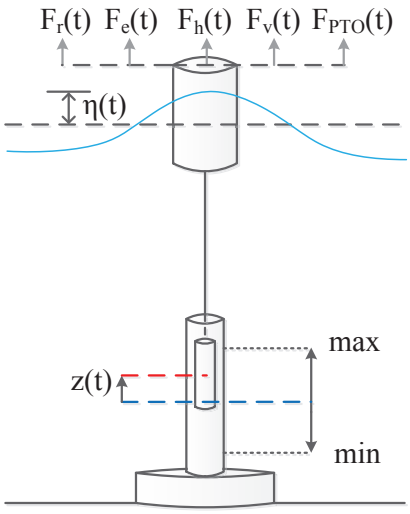

Fig. 1. System model with WEC and PTO

In this work, a cylindrical point absorber of mass M moving in heave motion is modelled. The model is based on linear wave theory but also includes the non-linear effect of viscosity. The hydrostatic force $F_h(t)$, the radiation force $F_r(t)$, the excitation force $F_e(t)$, the non-linear viscous force $F_v(t)$ and the controlled PTO force $F_{PTO}(t)$ as shown in Fig. 1, are all components of the hydrodynamic equation (1),

$$M\ddot{z}(t) = F_h(t) + F_r(t) + F_e(t) + F_v(t) + F_{PTO}(t) \quad (1)$$

The hydrodynamic system (1) is represented by the heave displacement $z(t)$, velocity $\dot{z}(t)$, the wave elevation $\eta(t)$ and the wave velocity $\dot{\eta}(t)$, where these are with respect to the equilibrium position. As this is a cylinder, the hydrostatic force is a linear function of the displacement $z(t)$, where β is the linear hydrostatic spring constant. The radiation force $F_r(t)$ is represented by a convolution integral from the Cummins transformation (Cummins, 1962), where the radiation kernel $h_r(t)$ and the added mass m_μ were found using WAMIT (Lee, 1995). The viscous force $F_v(t)$ is a non-linear component which depends on the relative velocity between the WEC and wave. The PTO force $F_{PTO}(t)$ is a force created by the control system. The non-linear mechanical model of the WEC is as follows,

$$\begin{aligned}(M+m_\mu)\,\ddot{z}(t) + \int_0^t h_r(\tau)\dot{z}(t-\tau)d\tau + \beta z(t) \\ +C_{vis}(t)\left(\dot{z}(t)-\dot{\eta}(t)\right) = (M+m_\mu)\left(u_q(t)+v(t)\right)\end{aligned} \quad (2)$$

where the scaled forces, $u_q(t)$ and $v(t)$ are,

$$u_q(t) = \frac{F_{PTO}(t)}{M+m_\mu} \qquad v(t) = \frac{F_e(t)}{M+m_\mu} \quad (3)$$

The excitation force $F_e(t)$ is a non-causal convolution integral of the wave elevation $\eta(t)$, where the excitation kernel $h_e(t)$ was found using WAMIT (Lee, 1995).

$$F_e(t) = \int_{-\infty}^t h_e(\tau)\eta(t-\tau)d\tau \quad (4)$$

The radiation kernel $h_r(t)$ can be expressed as a weighted sum of complex exponentials (5), where the parameters can be identified from the impulse response $h_r(t)$ using Prony's method,

$$h_r(t) \approx \tilde{h}_r(t) = c_1 e^{\mu_1 t} + c_2 e^{\mu_2 t} + c_3 e^{\mu_3 t} + ... + c_n e^{\mu_n t} \quad (5)$$

The radiation force, $F_r(t)$, can then be represented in the Laplace domain as $F_r(s) = sH_r(s)Z(s)$, where,

$$H_r(s) = \mathscr{L}\{\tilde{h}_r(t)\} = \frac{b_m s^m + b_{m-1}s^{m-1} + ... + b_0}{s^n + a_{n-1}s^{n-1} + ... + a_0} \quad (6)$$

A finite state space approximation can then be produced from (6), as;

$$\begin{aligned}\dot{\boldsymbol{x}}_{\boldsymbol{r}}(t) &= A_r \boldsymbol{x}_{\boldsymbol{r}}(t) + B_r \dot{z}(t) \\ F_r(t) &= C_r \boldsymbol{x}_{\boldsymbol{r}}(t) + D_r \dot{z}(t)\end{aligned} \quad (7)$$

where $\boldsymbol{x}_{\boldsymbol{r}}(t) \in \mathbb{R}^n$,$A_r \in \mathbb{R}^{n\times n}$,$B_r \in \mathbb{R}^n$,$C_r \in \mathbb{R}^{1\times n}$.

The non-linear viscosity force $F_v(t)$, is based on the semi-empirical Morison equation (Morison et al., 1950),

$$F_v(t) = -C_{vis}(t)\left(\dot{z}(t)-\dot{\eta}(t)\right) \quad (8)$$

where,

$$C_{vis}(t) = \frac{1}{2}\rho C_d A\left|\dot{z}(t)-\dot{\eta}(t)\right|.$$

Here ρ is the density of water, C_d is the drag coefficient (Bhinder et al., 2011) and A is the sectional area of the point absorber which is orthogonal to the direction of the force.

The non-linear hydrodynamic model (2) can then be represented in the state space form,

$$\frac{d}{dt}\begin{bmatrix} z(t) \\ \dot{z}(t) \\ \boldsymbol{x_r}(t) \end{bmatrix} = A_c(t)\begin{bmatrix} z(t) \\ \dot{z}(t) \\ \boldsymbol{x_r}(t) \end{bmatrix} + B_c u_q(t) + F_c v(t) + E_c(t)\dot{\eta}(t) \tag{9}$$

where,

$$A_c(t) = \begin{bmatrix} 0 & 1 & \mathbf{0} \\ -\frac{\beta}{M+m_\mu} & -\frac{(D_r+C_{vis}(t))}{M+m_\mu} & -\frac{C_r}{M+m_\mu} \\ 0 & B_r & A_r \end{bmatrix}$$

$$F_c = B_c = \begin{bmatrix} 0 \\ 1 \\ \mathbf{0} \end{bmatrix} \quad E_c(t) = \begin{bmatrix} 0 \\ \frac{C_{vis}(t)}{M+m_\mu} \\ \mathbf{0} \end{bmatrix} \quad \boldsymbol{x}(t) = \begin{bmatrix} z(t) \\ \dot{z}(t) \\ \boldsymbol{x_r}(t) \end{bmatrix} \tag{10}$$

2.2 Linear Permanent Magnet Generator PTO

In the following work, a Linear Permanent Magnet Generator (LPMG) (Polinder et al., 2004) is used to produce the PTO force, $F_{PTO}(t)$. Using this non-ideal PTO introduces resistive losses, which have to be included within the control optimisation to enable maximum electrical power generation. Following on from recent work (O'Sullivan and Lightbody, 2015, 2016a), this paper also uses a cascade control scheme; the slower outer MPC control loop sends piecewise linear PTO force reference points to the faster inner loop, where the Q axis current and hence the machine force is then controlled using a PI controller.

3. EFFECTS OF VISCOSITY ON POWER ABSORPTION

In previous work (O'Sullivan and Lightbody, 2016a), viscosity effects were not considered. Here, it is initially assumed that the MPC prediction model is linear as in (O'Sullivan and Lightbody, 2015) with no viscous modelling included. However, the non-linear simulation model includes viscosity as described in equations (8) and (9). The WEC used in this material is a cylindrical point absorber with a radius of 5 m and a draft of 10 m. A cascade control method is used, where the outer MPC control sends piecewise linear reference points to a faster inner control loop, where the PTO force is controlled using a faster sample time of $T_{gen} = 0.001$ s. The prediction horizon used is $N = 100$ with an outer sample time of $T_L = 0.1$ s, where the control horizon used is the same length as the prediction horizon. As shown in (O'Sullivan and Lightbody, 2016a), the MPC involves maximising an average electrical power (11) within the mechanical linear constraints (WEC heave, WEC velocity and PTO force), where this includes the resistive losses from the LPMG.

$$P_e = -\frac{1}{T}\int_{t=0}^{T}\left(\left(M+m_\mu\right)u_q(t)\dot{z}(t) + \frac{R}{\psi^2}u_q^2(t)\right)dt \tag{11}$$

where,

$$\psi = \frac{\lambda'_{fd}\frac{\pi}{\tau}}{M+m_\mu}$$

λ'_{fd}, τ and R are the flux linkage, the pole pitch and the resistance of the LPMG. The system was tested using monochromatic waves of amplitude 1 m, ranging between 0.219 rad/s and 1.23 rad/s. The linear MPC (O'Sullivan and Lightbody, 2016a) was tested on the system with and without constraints, where the system did and did not include the viscous forces. It is clear from Fig. 2 that the viscous force which is not accounted for in the linear MPC prediction model has a dramatic effect on the electrical power production. In fact, in this example, negative electrical power is produced over a wide frequency range. This points to the fact that the relative velocity between the device and the sea surface must be significant, hence causing a serious model mismatch. Some improvement in performance of the viscous system is obtained in the presence of the mechanical constraints, since it decreases the model mismatch by restricting the relative velocity. However, the power absorption across the frequency range is still unsatisfactory.

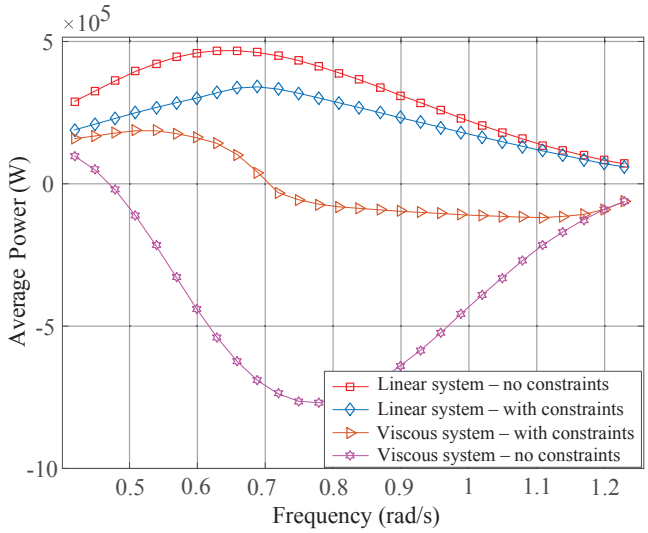

Fig. 2. Average electrical power produced from monochromatic waves with amplitude 1 m. A linear inviscid model is used within the MPC in each case. i) Linear inviscid system, without constraints ii) Linear inviscid system with constraints, iii) Non-linear viscous system with constraints, iv) Non-linear viscous system without constraints

3.1 Non-Linear Model Predictive Control

The inclusion of viscosity within the MPC model yields a non-linear MPC problem. In this work, a NLMPC, which is comparable to (Huzmezan and Maciejowski, 1998), is implemented. To simplify the optimisation problem, the prediction model is linearised at each step across the prediction horizon, using the predicted velocities obtained as the solution to the optimal control problem at the last control sample. By using predicted velocities, the non-linear viscous coefficient can then be linearised at each control sample (12) across the prediction horizon.

$$\tilde{\boldsymbol{C}}_{\boldsymbol{vis}}(k+i) = \rho C_d A\left|\dot{\boldsymbol{z}}^*(k+i|k-1) - \dot{\boldsymbol{\eta}}(k+i)\right)| \tag{12}$$

where $\dot{\boldsymbol{z}}^*(k+i|k-1)$ is the predicted velocity at the i^{th} step into the future, from the optimal state trajectory predicted as part of the solution for the controls at the $(k-1)^{th}$ sample. It is assumed here that the sea surface velocity $\dot{\boldsymbol{\eta}}(k+i)$ is known over the prediction horizon.

Using these predicted velocities, $\dot{\boldsymbol{z}}^*(k+i|k-1)$ and $\dot{\boldsymbol{\eta}}(k+i)$, the non-linear $A_c(t)$ and $E_c(t)$ matrices from (9) can then

be linearised at each control step over the horizon, as shown in (13)

$$\tilde{A}_c(k+i) = \begin{bmatrix} 0 & 1 & \mathbf{0} \\ -\frac{\beta}{M+m_\mu} & -\frac{(D_r+\tilde{C}_{vis}(k+i))}{M+m_\mu} & -\frac{C_r}{M+m_\mu} \\ 0 & B_r & A_r \end{bmatrix}$$
$$\tilde{E}_c(k+i) = \begin{bmatrix} 0 \\ \frac{\tilde{C}_{vis}(k+i)}{M+m_\mu} \\ \mathbf{0} \end{bmatrix} \quad (13)$$

The digitisation of the continuous model (9) was accomplished assuming a first order hold (FOH); integral action was also included. This results in the following discrete time, LPV prediction model,

$$\boldsymbol{x_b}(k+i+1) = A_b(k+i)\boldsymbol{x_b}(k+i) + B_b(k+i)\Delta u(k+i+1) + F_b(k+i)\Delta v(k+i+1) + E_b(k+i)\Delta\dot{\eta}(k+i+1)$$
$$\boldsymbol{y_b}(k+i+1) = C_b\boldsymbol{x_b}(k+i+1) \quad (14)$$

where $i \in \{0, 1, .., (N-1)\}$,

and

$$\boldsymbol{x_b}(k) = \begin{bmatrix} z(k) \\ \dot{z}(k) \\ \boldsymbol{x_r}(k) \\ u(k) \\ v(k) \\ \dot{\eta}(k) \end{bmatrix} \quad \boldsymbol{y_b}(k) = \begin{bmatrix} z(k) \\ \dot{z}(k) \\ u(k) \\ \dot{\eta}(k) \end{bmatrix}$$

$$A_b(k+i) = \left[\begin{array}{c|ccc} e^{\tilde{A}_c(k+i)T_L} & \Lambda_B(k+i) & \Lambda_B(k+i) & \Lambda_V(k+i) \\ \mathbf{0} & 1 & 0 & 0 \\ \mathbf{0} & 0 & 1 & 0 \\ \mathbf{0} & 0 & 0 & 1 \end{array}\right]$$

Here $A_b(k+i) \in \mathbb{R}^{(n+5)\times(n+5)}$,
$\Lambda_B(k+i) = \tilde{A}_c(k+i)^{-1}\left(e^{\tilde{A}_c(k+i)T_L} - I\right)B_c$
$\Gamma_B(k+i) = \frac{1}{T_L}\tilde{A}_c(k+i)^{-1}\left(\Lambda_B(k+i) - T_L B_c\right)$
Then using the linear approximation $\tilde{E}_c(k+i)$ from (13), the following can be constructed,

$$B_b(k+i) = \begin{bmatrix} \Gamma_B(k+i) \\ 1 \\ 0 \\ 0 \end{bmatrix} \in \mathbb{R}^{(n+5)\times 1}$$
$$F_b(k+i) = \begin{bmatrix} \Gamma_B(k+i) \\ 0 \\ 1 \\ 0 \end{bmatrix} \in \mathbb{R}^{(n+5)\times 1}$$
$$E_b(k+i) = \begin{bmatrix} \Gamma_V(k+i) \\ 0 \\ 0 \\ 1 \end{bmatrix} \in \mathbb{R}^{(n+5)\times 1}$$

where, $\Lambda_V(k+i) = \tilde{A}_c(k+i)^{-1}\left(e^{\tilde{A}_c(k+i)T_L} - I\right)\tilde{E}_c(k+i)$
$\Gamma_V(k+i) = \frac{1}{T_L}\tilde{A}_c(k+i)^{-1}\left(\Lambda_V(k+i) - T_L\tilde{E}_c(k+i)\right)$

The following prediction equation can be formed to predict the output vector at the k^{th} sample over the N steps of the prediction horizon,

$$\hat{\boldsymbol{Y}}(k) = P\boldsymbol{x_b}(k) + G\boldsymbol{\Delta U}(k) + H\boldsymbol{\Delta V}(k) + M\boldsymbol{\Delta\dot{\eta}}(k), \quad (15)$$

where $\hat{\boldsymbol{Y}}(k) \triangleq \left[\boldsymbol{y_b}(k+1|k)^T .....\boldsymbol{y_b}(k+N|k)^T\right]^T$ and $\boldsymbol{\Delta U}(k)$, $\boldsymbol{\Delta V}(k)$ and $\boldsymbol{\Delta\dot{\eta}}(k)$ have the same structure.

$P \in \mathbb{R}^{4N\times(n+5)}$, $G \in \mathbb{R}^{4N\times N}$, $H \in \mathbb{R}^{4N\times N}$ and $M \in \mathbb{R}^{4N\times N}$,

$$P = \begin{bmatrix} C_b A_b(k) \\ C_b\boldsymbol{\Phi}_1 A_b(k) \\ \vdots \\ C_b\boldsymbol{\Phi}_{N-1}A_b(k) \end{bmatrix},$$

$$H = \begin{bmatrix} C_bB_b(k) & 0 & .. & 0 \\ C_b\boldsymbol{\Phi}_1B_b(k) & C_bB_b(k+1) & .. & 0 \\ \vdots & \vdots & \ddots & \vdots \\ C_b\boldsymbol{\Phi}_{N-1}B_b(k) & C_b\boldsymbol{\Phi}_{N-2}B_b(k+1) & .. & C_bB_b(k+N-1) \end{bmatrix} \quad (16)$$

Here G, H and M have a similar structure to H (16) and $\boldsymbol{\Phi}_n \triangleq A_b(k+n)...A_b(k+2)A_b(k+1)$,

As shown in previous work (O'Sullivan and Lightbody, 2016a), by using (15), a cost function (17) can be formed. By minimising this cost function with the incorporation of the linear constraints, the optimal $\boldsymbol{\Delta u}(k+i|k)$ values can be found; these optimal values allow maximum power absorption.

$$J = \frac{1}{2}\boldsymbol{\Delta U}^T G^T Q G\boldsymbol{\Delta U} + \boldsymbol{\Delta U}^T G^T Q\left(P\boldsymbol{x_b} + H\boldsymbol{\Delta V} + M\boldsymbol{\Delta\dot{\eta}}\right) + \frac{1}{2}\left(P\boldsymbol{x_b} + H\boldsymbol{\Delta V} + M\boldsymbol{\Delta\dot{\eta}}\right)^T Q\left(P\boldsymbol{x_b} + H\boldsymbol{\Delta V} + M\boldsymbol{\Delta\dot{\eta}}\right) \quad (17)$$

Simulation Results This non-linear viscid hydrodynamic system was then tested with the NLMPC algorithm with and without linear mechanical constraints. To provide reference results showing the optimal electrical power extraction that is available, the models in the simulation and controller are matched. The system was tested under multiple sea states, with the significant height and mean wave period selected for each sea state. Each sea state was implemented using a Bretschneider spectrum, which produced irregular waveforms. It was assumed that the future excitation waveforms were known for the finite horizon, with $N = 100$ and an outer sampling period of $T_L = 0.1s$,

It is shown in Fig.3 that the NLMPC succeeds in producing positive average electrical power, unlike the previous case in which there was no viscosity term in the MPC model (Fig. 2). When the NLMPC with and without constraints are compared, it is shown that the impact of the linear constraints on the absorbed average electrical power is insignificant until the seventh sea state ($T_{avg} = 13.326$ s $H_s = 4.5$ m) . From the seventh sea state, the PTO force is then used from time to time to prevent the system from operating outside the feasible region in the near future, hence, reducing the average electrical power from the unconstrained maximum.

The NLMPC produces promising results, but at the cost of increased computational effort where the NLPMC uses approximately 5 times the computational time of the linear MPC for the unconstrained case and 2.5 times the

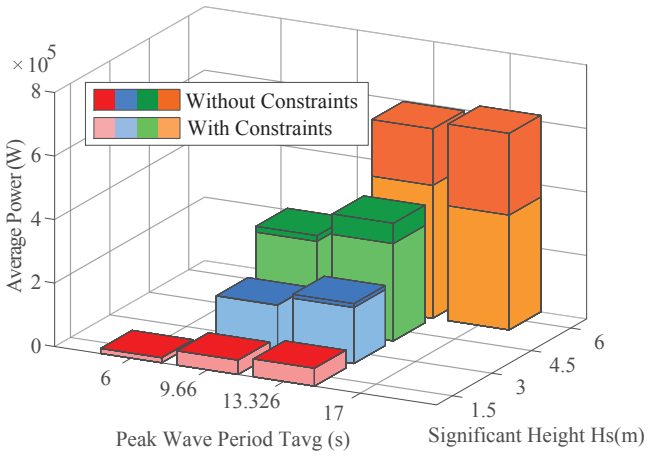

Fig. 3. NL-MPC Monte Carlo test results of the average electrical power absorbed from irregular waves using a Bretschneider spectrum with a range of different peak wave periods and significant heights

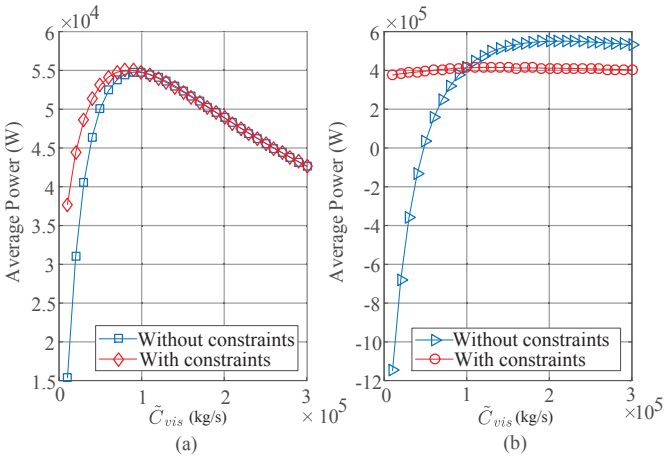

Fig. 4. Linear MPC performance with and without constraints. Average electrical power absorbed from (a) sea state 3 ($T_s = 13.326$ s $H_s = 1.5$ m), (b) sea state 8 ($T_s = 13.326$ s $H_s = 6$ m) using a Bretschneider spectrum

computational time when constraints are included. A more efficient method for dealing with the viscous forces in the MPC model would be a linear MPC which includes a linear estimation of the non-linear viscosity force, which could be fine tuned for each sea state.

3.2 Linear Viscid Model Predictive Control

The linear viscid Model Predictive Controller is used to approximate the NLMPC, where the linear viscous coefficient estimate ($\tilde{C}_{vis}$) is chosen to produce similar average electrical power at each sea-state as the NLMPC, but without the computational complexity. Here a constant $\tilde{C}_{vis}$ is selected for each sea-state, to provide constant matrices $\tilde{A}_c$ and $\tilde{E}_c$ as defined in (13). Hence, for a given sea-state this represents a linear MPC problem.

The results in Fig. 4 show, how the electrical power extracted depends on the choice of $\tilde{C}_{vis}$. Here the MPC system was tested for sea state 3 ($T_{avg} = 13.326$ s $H_s = 1.5$ m) and sea state 8 ($T_{avg} = 13.326$ s $H_s = 6$ m), with and without constraints. There is unique $\tilde{C}_{vis}$ value that corresponds to the maximum extractable average electrical power; the optimum $\tilde{C}_{vis}$ value during sea state 3 is 1×10^5 kg/s and the optimum $\tilde{C}_{vis}$ value during sea state 8 is 2.1×10^5 kg/s.

When the linear constraints are included in the MPC, the relative velocity between the wave and WEC is restricted, especially at higher sea states where the WEC velocity constraints are frequently active. This relative velocity restriction causes the average electrical power to be insensitive to choices of $\tilde{C}_{vis}$ at sea states.

The linear MPC, with and without constraints, was tested across the entire sea state range, where the optimum $\tilde{C}_{vis}$ values corresponding to the maximum average power points are shown in Fig. 5. This also shows the $\tilde{C}_{vis}$ regions where the average power is above 98% of the maximum average power available ($\tilde{\boldsymbol{C}}_{\boldsymbol{vis98\%}}$).

From Fig. 5 the optimal $\tilde{C}_{vis}$ value with constraints increases some what proportionally with the corresponding sea state, but at a much reduced rate than when constraints were not included. It is also shown that when the constraints are included, the $\tilde{\boldsymbol{C}}_{\boldsymbol{vis98\%}}$ regions broaden, which then causes a larger common $\tilde{\boldsymbol{C}}_{\boldsymbol{vis98\%}}$ overlap across the sea states. Therefore, a sea state invariant $\tilde{C}_{vis}$ estimate value can be found, which allows the average electrical power for all sea states to operate between 96% to 100% of the maximum power available, hence, allowing a simple and efficient way of sub-optimally extracting acceptable electrical power. In this example, when the constraints are included, a constant $\tilde{C}_{vis} = 1 \times 10^5$ kg/s would provide between $96 - 100\%$ of the average electrical power extracted by optimally tuning $\tilde{C}_{vis}$ for each sea-state.

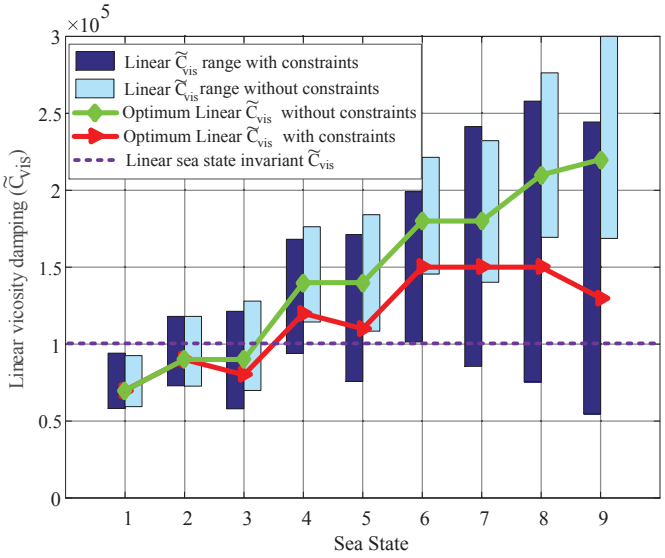

Fig. 5. The linear $\tilde{C}_{vis}$ range of the maximum available by optimal choice of $\tilde{C}_{vis}$ that produces an average power between 98% and 100%, $\tilde{\boldsymbol{C}}_{\boldsymbol{vis98\%}}$ with and without constraints is shown. Furthermore, the optimum linear $\tilde{C}_{vis}$ is given for each sea-state.

4. DISCUSSION

The performance of the system under NLMPC, linear MPC (with optimal $\tilde{C}_{vis}$ selected for each sea-state) and a linear MPC with constant linear viscous damping ($\tilde{C}_{vis} = 1 \times 10^5$ kg/s) was compared over the 9 sea states as defined in Fig. 3. In Fig. 6, it is shown that in the unconstrained case, the average electrical power produced between the NLMPC and the linear MPC (with optimal $\tilde{C}_{vis}$ selected for each sea-state) is similar up to sea-state 7. Furthermore, the average electrical powers produced when using the linear MPC with constant linear viscous damping ($\tilde{C}_{vis} = 1 \times 10^5$ kg/s) diverged from the NLMPC average electrical powers as the sea-state increased.

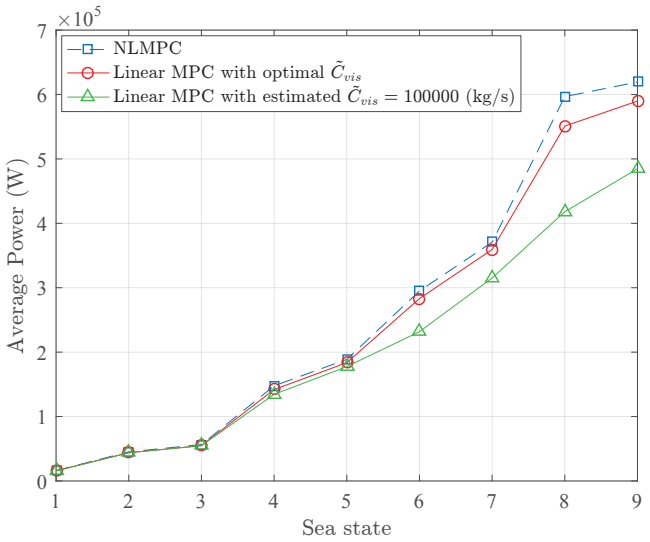

Fig. 6. A comparison of the average electrical powers found without constraints using i) NLMPC, ii) Linear MPC, where the optimally tuned $\tilde{C}_{vis}$ estimations are used and iii) Linear MPC, with a sea state invariant $\tilde{C}_{vis} = 100000$ (kg/s) which is constant for all sea states.

When examining the constrained case, as shown in Fig. 7, it is important to note that all three controllers provided similar average electrical power extraction, except at the energetic sea-state 9. This implies that mechanical constraints in this example, limit the relative velocity and allow for excellent performance of the linear MPC, with a fixed linear viscous damping model.

5. CONCLUSION

In this work, the negative effects of the non-linear viscosity on the average electrical power absorption when using an inviscid MPC model was shown. With the inclusion of linear constraints in the optimisation, the mismatch between the control and system model and hence the performance was marginally improved.

A LPV NLPMC was then implemented in simulation with a matched model, which produced the reference performance where maximum electrical power was produced. The NLMPC performance came with increased computational complexity. To decrease the computational complexity, a linear damping viscosity model was incorporated

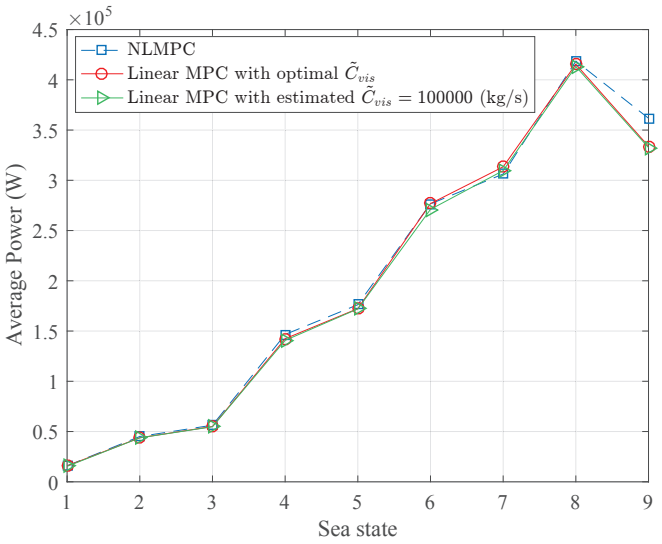

Fig. 7. A comparison of the average electrical powers found with constraints using i) NLMPC, ii) Linear MPC, where the optimally tuned $\tilde{C}_{vis}$ estimations are used and iii) Linear MPC, with a sea state invariant $\tilde{C}_{vis} = 100000$ which is constant for all sea states.

into the linear MPC. It was found that when the $\tilde{C}_{vis}$ value was tuned for each individual sea state, the average power collected was comparable to the results produced using the NLMPC.

By introducing linear mechanical constraints in the MPC optimisation, it was shown that the average power was less sensitive to the choice of $\tilde{C}_{vis}$ than for the unconstrained case. In fact a constant sea-state invariant $\tilde{C}_{vis}$ could be used to create a system which could extract between 96% and 100% of the electrical power obtained with the optimal $\tilde{C}_{vis}$ per sea-state. Comparing the results from the NLMPC and the linear MPC approximations, it is shown that the inclusion of the linear constraints within the optimisation cause a convergence of the performance across all three controllers. From this, it can be said that with the help of linear constraints, satisfactory power maximisation can be accomplished, via MPC, with the inclusion of a single simple linear drag coefficient $\tilde{C}_{vis}$, without the complexity associated with NLPMC.

ACKNOWLEDGEMENTS

This work was supported by the SFI Centre for Marine Renewable Energy Research (12/RC/2302).

REFERENCES

Abraham, E. and Kerrigan, E.C. (2013). Optimal active control and optimization of a wave energy converter. *IEEE Transactions on Sustainable Energy*, 4, 324–332.

Aubry, J., Ahmed, H.B., and Multon, B. (2012). Sizing optimization methodology of a surface permanent magnet machine-converter system over a torque-speed operating profile: Application to a wave energy converter. *IEEE Transactions on Industrial Electronics*, 59(5), 2116–2125.

Babarit, A., Duclos, G., and Clément, A.H. (2004). Comparison of latching control strategies for a heaving wave

energy device in random sea. *Applied Ocean Research*, 26(5), 227–238.

Bhinder, M., Babarit, A., Gentaz, L., and Ferrant, P. (2011). Assessment of viscous damping via 3d-cfd modelling of a floating wave energy device. In *9th European Wave and Tidal Energy Conference*.

Budal, K. and Falnes, J. (1975). A resonant point absorber of ocean-wave power. *Nature*, 256, 478.

Budal, K. and Falnes, J. (1977). Optimum operation of improved wave-power converter. *Marine Science Communications*, 3, 133–150.

Budal, K. and Falnes, J. (1980). Interacting point absorbers with controlled motion. In *Power from Sea Waves*, 381–399.

Clément, A., McCullen, P., Falcão, A., Fiorentino, A., Gardner, F., Hammarlund, K., Lemonis, G., Lewis, T., Nielsen, K., Petroncini, S., and Others (2002). Wave energy in Europe: current status and perspectives. *Renewable and sustainable energy reviews*, 6(5), 405–431.

Cretel, J., Lightbody, G., Thomas, G.P., and Lewis, A.W. (2011). Maximisation of energy capture by a wave-energy point absorber using model predictive control. In *IFAC Proceedings Volumes (IFAC-PapersOnline)*, volume 18, 3714–3721.

Cretel, J.A.M., Lewis, A.W., Lightbody, G., and Thomas, G.P. (2010). An Application of Model Predictive Control to a Wave Energy Point Absorber. In *Proceedings of the IFAC Conference on Control Applications in Marine Systems*, 1980, 1–6.

Cummins, W.E. (1962). The Impulse Response Function and Ship Motions. *Schiffstechnik*, 9, 101–109.

Drew, B., Plummer, A.R., and Sahinkaya, M.N. (2009). A review of wave energy converter technology. *Proceedings of the Institution of Mechanical Engineers, Part A: Journal of Power and Energy*, 223(8), 887–902.

Fusco, F. and Ringwood, J. (2011). Suboptimal causal reactive control of wave energy converters using a second order system model. In *Proceedings of the 21st (2011) International Offshore and Polar Engineering Conference*, 687–694. International Society of Offshore and Polar Engineers (ISOPE).

Fusco, F. and Ringwood, J.V. (2010). Short-term wave forecasting for real-time control of wave energy converters. *IEEE Transactions on Sustainable Energy*, 1, 99–106.

Fusco, F. and Ringwood, J.V. (2013). A Simple and Effective Real-Time Controller for Wave Energy Converters. *IEEE Transactions on Sustainable Energy*, 4(1), 21–30.

Garcia-Rosa, P.B. and Ringwood, J.V. (2016). On the sensitivity of optimal wave energy device geometry to the energy maximizing control system. *IEEE Transactions on Sustainable Energy*, 7(1), 419–426.

Giorgi, G., Pe, M., and Ringwood, J.V. (2016). Nonlinear Hydrodynamic Models for Heaving Buoy Wave Energy Converters. In *Asian Wave and Tidal Energy Conference*, 144–153.

Guérinel, M., Alves, M., and Sarmento, A. (2011). Nonlinear modelling of the dynamics of a free floating body. *EWTEC, Southampton*.

Hals, J., Falnes, J., and Moan, T. (2011). Constrained optimal control of a heaving buoy wave-energy converter. *Journal of Offshore Mechanics and Arctic Engineering*, 133(1), 11401.

Huzmezan, M. and Maciejowski, J. (1998). Reconfiguration and scheduling in flight using quasi-LPV high-fidelity models and MBPC control. In *American Control Conference, 1998. Proceedings of the 1998*, volume 6, 3649–3653 vol.6.

Lee, C.H. (1995). *WAMIT Theory Manual*. Dept. of Ocean Eng. , MIT.

Lenee-Bluhm, P., Paasch, R., and Özkan-Haller, H.T. (2011). Characterizing the wave energy resource of the US Pacific Northwest. *Renewable Energy*, 36(8), 2106–2119.

Lovelace, E.C., Jahns, T.M., and Lang, J.H. (2000). Impact of saturation and inverter cost on interior PM synchronous machine drive optimization. *IEEE Transactions on Industry Applications*, 36(3), 723–729.

Maciejowski, J.M. (2002). *Predictive Control: with Constraints*. Pearson Education. Prentice Hall.

Molinas, M., Skjervheim, O., Andreasen, P., Undeland, T., Hals, J., Moan, T., and Sorby, B. (2007). Power electronics as grid interface for actively controlled wave energy converters. In *2007 IEEE International Conference on Clean Electrical Power*, 188–195.

Montoya Andrade, D.E., De La Villa Jaén, A., and García Santana, A. (2014). Considering linear generator copper losses on model predictive control for a point absorber wave energy converter. *Energy Conversion and Management*, 78, 173–183.

Morison, J.R., Johnson, J.W., Schaaf, S.A., and Others (1950). The force exerted by surface waves on piles. *Journal of Petroleum Technology*, 2(05), 149–154.

O'Sullivan, A.C. and Lightbody, G. (2015). Wave to Wire Power Maximisation from a Wave Energy Converter. In *In Proceedings of the 11th European Wave and Tidal Energy Conference (EWTEC)*. Nantes.

O'Sullivan, A.C. and Lightbody, G. (2016a). Co-design of a wave energy converter using constrained predictive control. *Renewable Energy*, 102, 142–156.

O'Sullivan, A.C. and Lightbody, G. (2016b). Predictive control of a wave to wire energy conversion system - the importance of field weakening. In *UKACC*.

Paparella, F. and Ringwood, J.V. (2016). Optimal control of a three-body hinge-barge wave energy device using pseudo-spectral methods. *IEEE Transactions on Sustainable Energy*, PP(99), 1.

Penalba Retes, M., Mérigaud, A., Gilloteaux, J.C., and Ringwood, J. (2015). Nonlinear Froude-Krylov force modelling for two heaving wave energy point absorbers. In *Proceedings of the 11th European Wave and Tidal Energy Conference*. European Wave and Tidal Energy Conference 2015.

Polinder, H., Damen, M.E.C., and Gardner, F. (2004). Linear PM Generator System for Wave Energy Conversion in the AWS. *IEEE Transactions on Energy Conversion*, 19(3), 583–589.

Schoen, M.P., Hals, J., and Moan, T. (2011). Wave prediction and robust control of heaving wave energy devices for irregular waves. *IEEE Transactions on Energy Conversion*, 26(2), 627–638.

Tedeschi, E., Carraro, M., Molinas, M., and Mattavelli, P. (2011). Effect of control strategies and power take-off efficiency on the power capture from sea waves. *IEEE Transactions on Energy Conversion*, 26(4), 1088–1098.